Proceedings of the American Control Conference
San Diego, California • June 1999

Robustness of ARMARKOV Adaptive Control Disturbance Rejection Algorithm

Harshad S. Sane, Ravinder Venugopal and Dennis S. Bernstein [1]
Department of Aerospace Engineering, The University of Michigan, Ann Arbor, MI.

1 Introduction

In this paper we investigate the properties of the ARMARKOV adaptive control (AAC) method developed for disturbance rejection applications [4]. The theoretical foundation of AAC is based upon three key elements. First, the underlying model structure of AAC is the ARMARKOV model, which is a structurally constrained ARMA model with explicit Markov parameters which has been shown to be resistant to the effects of measurement noise [1]. Next, AAC utilizes a controller update procedure that is based upon measured data and which requires a model of only the secondary path transfer function (from the control input to the error variables). Finally, for controller update AAC employs a variable step size that is guaranteed to decrease the distance from the current controller to an ideal controller at each update.

AAC was developed specifically for active noise and vibration control applications and has been implemented experimentally on laboratory-scale experiments to suppress wide range of disturbances [4]. To provide insight into the properties of AAC this paper presents the results of a numerical study which investigates the ability of the adaptive controller to recover performance in the face of plant and disturbance spectrum changes such as modeling uncertainty in the secondary path transfer function (control input to performance variable) and tonal disturbances with changing frequency.

Next we consider the ability of the algorithm to adapt to changes that can threaten to destabilize the closed-loop system such as abrupt plant changes that involve perturbations to the loop transfer function which can violate the Nyquist criterion. These features are of special interest in view of the fact that the algorithm neither requires nor utilizes a model of the feedback transfer function.

2 ARMARKOV/Toeplitz Models of Systems

Consider the linear discrete-time system

$$x(k+1) = Ax(k) + Bu(k) + D_1 w(k), \quad (1)$$
$$z(k) = E_1 x(k) + E_2 u(k) + E_0 w(k), \quad (2)$$
$$y(k) = Cx(k) + Du(k) + D_2 w(k). \quad (3)$$

The *disturbance* $w(k)$, the *control* $u(k)$, the *measurement* $y(k)$ and the *performance* $z(k)$ are in $\mathcal{R}^{m_w}, \mathcal{R}^{m_u}, \mathcal{R}^{l_y}$ and $\mathcal{R}^{l_z}$, respectively. The objective of the standard problem is to determine a controller G_c that produces a control signal $u(k) = G_c y(k)$ such that a performance measure involving $z(k)$ is minimized.

Next we write the ARMARKOV/Toeplitz model of (1) - (3) [4] as

$$Z(k) = W_{zw}\Phi_{zw}(k) + B_{zu}U(k), \quad (4)$$
$$Y(k) = W_{yw}\Phi_{yw}(k) + B_{yu}U(k). \quad (5)$$

Here W_{zw}, W_{yw}, B_{zu} and B_{yu} are the block-Toeplitz as defined in [4]. The *extended performance vector* $Z(k)$, the *extended measurement vector* $Y(k)$ and the *extended control vector* $U(k)$ are defined as [4]

$$Z(k) \triangleq [\, z(k) \quad \cdots \quad z(k-p+1) \,]^{\mathrm{T}},$$
$$Y(k) \triangleq [\, y(k) \quad \cdots \quad y(k-p+1) \,]^{\mathrm{T}},$$
$$U(k) \triangleq [\, u(k) \quad \cdots \quad u(k-p_c+1) \,]^{\mathrm{T}}, \quad (6)$$

where $p_c \triangleq \mu + n + p - 1$, p is a positive integer. The *ARMARKOV regressor vectors* $\Phi_{zw}(k)$ and $\Phi_{yw}(k)$ are given by

$$\Phi_{zw}(k) \triangleq [\, z(k-\mu) \quad \cdots \quad z(k-\mu-p-n+2) \quad w(k) \quad \cdots \quad w(k-\mu-p-n+2) \,]^{\mathrm{T}},$$
$$\Phi_{yw}(k) \triangleq [\, y(k-\mu) \quad \cdots \quad y(k-\mu-p-n+2) \quad w(k) \quad \cdots \quad w(k-\mu-p-n+2) \,]^{\mathrm{T}}. \quad (7)$$

Remark 1 Consider the nth-order discrete-time finite-dimensional linear time-invariant system

$$x(k+1) = Ax(k) + Bu(k), \quad (8)$$
$$y(k) = Cx(k) + Du(k), \quad (9)$$

The *ARMARKOV transfer function* of (8)-(9) is given by

$$G(z) = \frac{\sum_{j=1}^{\mu} H_{j-2} z^{n-j+\mu} + \sum_{i=1}^{n} \mathcal{B}_i z^{n-i}}{z^{\mu+n-1} + \alpha_1 z^{n-1} + \cdots + \alpha_n}. \quad (10)$$

where $\alpha_j \in \mathcal{R}$ and $\mathcal{B}_j \in \mathcal{R}^{l_y \times m_u}$ and the Markov parameters are defined as $H_{-1} \triangleq D$ and $H_j \triangleq CA^jB$ for $j \geq 0$. This system representation is nonminimal, overparametrized and constrained since the numerator and denominator of the transfer function are polynomials of order $\mu + n - 1$, and the coefficients of the terms $z^{\mu+n-2}$ through z^n in the denominator are zero. □

[1] This research was supported in part by the Air Force Office of Scientific Research under grant F49620-98-1-0037 and the University of Michigan Office of the Vice President for Research.

0-7803-4990-6/99 $10.00 © 1999 AACC

3 ARMARKOV Adaptive Control

The ARMARKOV/Toeplitz representation of the controller of order n_c and μ_c Markov parameters is given by

$$U(k) = \sum_{i=1}^{p_c} L_i \theta(k-i+1) R_i \Phi_{uy}(k). \quad (11)$$

Here we define the *controller parameter block vector* $\theta(k)$ and the regressor vector $\Phi_{uy}(k)$ as

$$\theta(k) \triangleq [-\alpha_{c,1}(k) I_{m_u} \quad \cdots \quad -\alpha_{c,n_c}(k) I_{m_u} \quad H_{c,0}(k) \quad \cdots \quad H_{c,\mu_c-2}(k) \quad \mathcal{B}_{c,1}(k) \quad \cdots \quad \mathcal{B}_{c,n_c}(k)]. \quad (12)$$

$$\Phi_{uy}(k) \triangleq [u(k-\mu_c) \quad \cdots \quad u(k-\mu_c-n_c-p_c+2) \quad y(k-1) \quad \cdots \quad y(k-\mu_c-n_c-p_c+2)]^T, \quad (13)$$

where $H_{c,j}$ are the Markov parameters of the controller and $\alpha_{c,i}(k)$ are parameters associated with the μ_c-ARMARKOV model of the controller. L_i and R_i are constraint matrices consisting of 1's and 0's preserving the block-Toeplitz structure. Thus from (4) and (11) we obtain

$$Z(k) = W_{zw}\Phi_{zw}(k) + B_{zu}\sum_{i=1}^{p_c} L_i\theta(k-i+1)R_i\Phi_{uy}(k). \quad (14)$$

Next, we define a cost function that evaluates the performance of the current value of $\theta(k)$ based upon the behavior of the system during the previous p_c steps. Therefore, we define the estimated performance $\hat{Z}(k) \triangleq W_{zw}\Phi_{zw}(k) + B_{zu}\sum_{i=1}^{p_c} L_i\theta(k)R_i\Phi_{uy}(k)$ and the estimated performance cost function $J(k) = \frac{1}{2}\hat{Z}^T(k)\hat{Z}(k)$.

The cost function $J(k)$ is minimized by updating the controller parameter vector $\theta(k)$ assuming that a minimizer θ^* exists [4]. The gradient of $J(k)$ with respect to $\theta(k)$ is given by

$$\frac{\partial J(k)}{\partial \theta(k)} = \sum_{i=1}^{p_c} L_i^T B_{zu}^T \hat{Z}(k) \Phi_{uy}^T(k) R_i^T, \quad (15)$$

which is used to update $\theta(k)$ using

$$\theta(k+1) = \theta(k) - \eta(k)\frac{\partial J(k)}{\partial \theta(k)}, \quad (16)$$

where $\eta(k)$ is the adaptive step size given by $\eta(k) = 1/(p_c\|B_{zu}\|_F^2\|\Phi_{uy}(k)\|_2^2)$. It is shown in [4] that the update law (16) with the step size $\eta(k)$ brings $\theta(k)$ closer to the minimizer θ^* of $J(k)$ with each time step. Note that, for implementing the algorithm in practice ((15), (16), $\eta(k)$) we only need know the secondary feedback matrix B_{zu} apart from the measurements z and y.

4 Acoustic Duct Model and Nominal Plant Simulations

The numerical simulations are based upon a 5 mode (10th order) acoustic duct model derived using modal decomposition of the acoustic response of the duct to external acoustic inputs [3]. The duct (length 6 ft) has two inputs, namely the disturbance speaker situated at $x = 0.2$ and a control speaker situated at $x = 5.8$, x being the coordinate along the length of the duct. The sensors y and z are situated at $x = 0.1$ and $x = 5.9$ respectively. The modal frequencies are equally spaced at 85Hz, 170Hz, 255Hz, 340Hz,and 425Hz and have an effective damping of 5%.

Consider nominal plant. The matrix B_{zu} is constructed using the algorithm discussed in [1] with the parameters $n = 10, \mu = 25$ and $p = 5$ with a sampling frequency of 2.0 KHz. The AAC algorithm is programmed in C in the form of a SIMULINK S-Function for use with MATLAB. The simulations are performed for three kinds of disturbances: single-tone, dual-tone and broadband. The controller parameters chosen for adaptation are $n_c = 10, \mu_c = 25$. For all simulations $\theta(k)$ is initialized to zero. Results for nominal plant are presented in Figure 1 through Figure 8 and the explanations for each figure are given below.

1. **Figure 1, 2 and 3 :** Consider single-tone disturbance at 320 Hz. Figure 1 shows open-loop and closed-loop time response. The controller successfully (bode plot in Figure 2) rejects the disturbance by adapting itself to an internal model controller with high gain at the disturbance frequency. The uniform placement of the poles and zeros of the controller (z-domain pole-zero map in Figure 3), attributed to the ARMARKOV structure (see remarks following (10)), provide the controller with a number of inherent anti-notches. The pole-zero pairs close to the disturbance frequency are automatically tuned so as to provide the internal model.
2. **Figure 4, 5:** Consider dual-tone disturbance (190 Hz and 320 Hz). The controller adapts to an internal model controller to reject both tones.
3. **Figure 6:** Consider white noise disturbance. The controller utilizes high gain and achieves up to 10 dB rejection of broad-band disturbance.
4. **Figure 7, 8:** Consider single-tone disturbance with frequency change (from 320 Hz to 190 Hz at $t \approx 1.3$). After a small period of adaptation the new disturbance is rejected. Bode plots of the controller before and after frequency change show that the algorithm converges such that the original peak (high gain at 320 Hz) is kept unchanged. Hence, the algorithm 'remembers' the previous disturbance. The 'memory' of the controller can be increased by choosing a larger value of μ_c.

5 Perturbed Plant Simulations

In this section we present the numerical simulations that were performed to investigate the properties of AAC algorithm. Figure 9 through Figure 14 present the results of the simulations. Explanations for the figures are provided below.

1. **Figure 9:** In this simulation we use a perturbed B_{zu} matrix in the gradient update (15, 16) and the nominal plant model. (a) single-tone disturbance rejection. (b) dual-tone disturbance rejection (c) broadband disturbance rejection.

2. **Figure 10:** In this simulation we use the perturbed plant model (modal frequencies are perturbed by $\pm 20\%$) and a perturbed B_{zu} matrix in equation (15), (16) (as in Figure 9) along with zero-mean Gaussian measurement noise. The signal-to-noise ratio is chosen to be 1.5. (a) single-tone disturbance rejection.(b) dual-tone disturbance rejection.

3. **Figure 11:** In this simulation, in addition to plant perturbation, inaccurate B_{zu} and measurement noise (as in Figure 10), we limit the control authority by saturating the control u, such that $|u| \leq u_{\max} = 2$. The plots show results for a dual-tone disturbance. (a) closed loop performance z. (b) Saturated control input u.

4. **Figure 12:** In this simulation we use a B_{zu} matrix generated for a 2-mode model of the same duct in the gradient update (15), (16) with the nominal 5-mode system. (a) performance with single-tone disturbance (b) performance with dual-tone disturbance (c) performance with broadband disturbance.

5. **Figure 13, 14:** In this simulation we destabilize the system by changing the feedback sign at an arbitrarily chosen time ($t = 0.3$ sec) and allow the controller to adapt so as to re-stabilize the closed-loop system and reject external disturbances. (a) single-tone disturbance rejection (b) dual-tone disturbance rejection. Figure 14 shows the poles of the closed loop system (in z-domain just after changing the feedback sign (denoted by $*$) and their ultimate locations after the controller adapts to a stabilizing controller (denoted by $\diamond$).

6 Conclusion

In this paper we performed numerical experiments involving the ARMARKOV adaptive control algorithm. The performance of the algorithm was considered under a diverse set of conditions representing plant and disturbance uncertainty including perturbed disturbance spectrum, perturbed plant model, additive measurement noise, control input saturation, and feedback path sign inversion. These numerical experiments can be viewed as only representative illustrations of the properties of this adaptive control algorithm. Nevertheless, these simulations suggest that the algorithm has significant ability to provide robust stability and performance under diverse deteriorating conditions.

References

[1] J. C. Akers and D. S. Bernstein, "Time-Domain Identification Using ARMARKOV/Toeplitz Models," *Proc. Amer. Contr. Conf.*, Albuquerque, NM, pp. 191-195, June 1997.

[2] K. J. Astrom and B. Wittenmark, *Adaptive Control*, 2nd edition, Reading, MA: Addison-Wesley, 1995.

[3] R. Venugopal and D. S. Bernstein, "State Space Modeling of Acoustic Duct with End-Mounted Speaker," *AME Trans. J. Vibr. Acoust.*, Vol. 120, pp. 770-775, 1998.

[4] R. Venugopal and D. S. Bernstein, "Adaptive Disturbance Rejection using ARMARKOV System Representations," *Proc. IEEE Conf. Dec. Contr.*, San Diego, CA, pp. 1884-1889, December 1997.

[5] H. Sane and D. S. Bernstein, "Active Noise Control Using an Acoustic Servovalve," *Proc. Amer. Contr. Conf.*, pp. 2621-2625, Philadelphia, PA, June 1998.

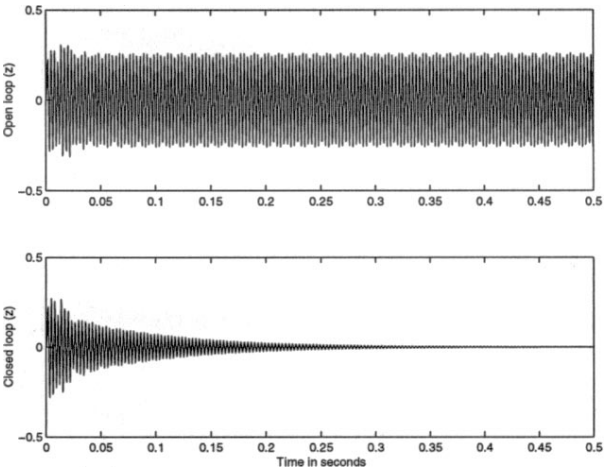

Figure 1: Open-loop and closed-loop response of the 5-mode acoustic duct to a sinusoidal disturbance at 320 Hz.

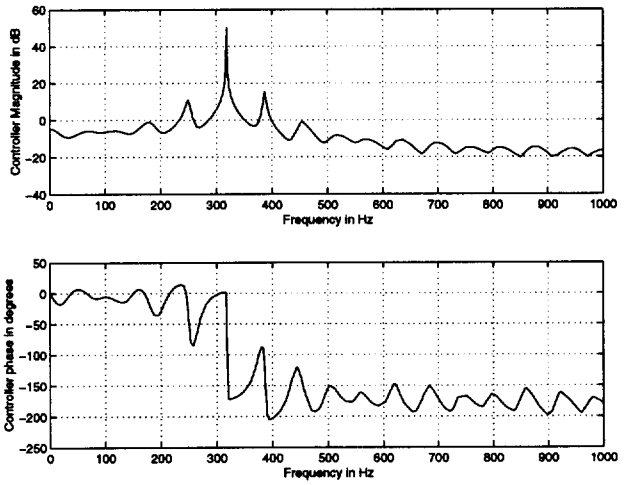

Figure 2: Bode plot of the adapted controller for a sinusoidal disturbance at 320 Hz.

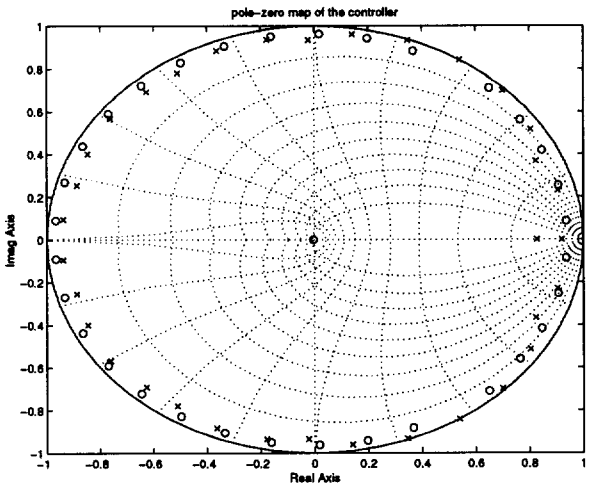

Figure 3: z-domain pole-zero plot of the adapted controller for a sinusoidal disturbance at 320 Hz.

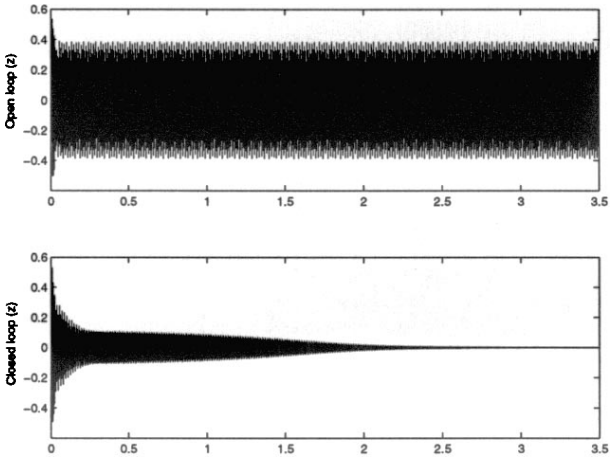

Figure 4: Open-loop and closed-loop response of the 5-mode acoustic duct to a dual-tone disturbance (190 Hz, 320 Hz).

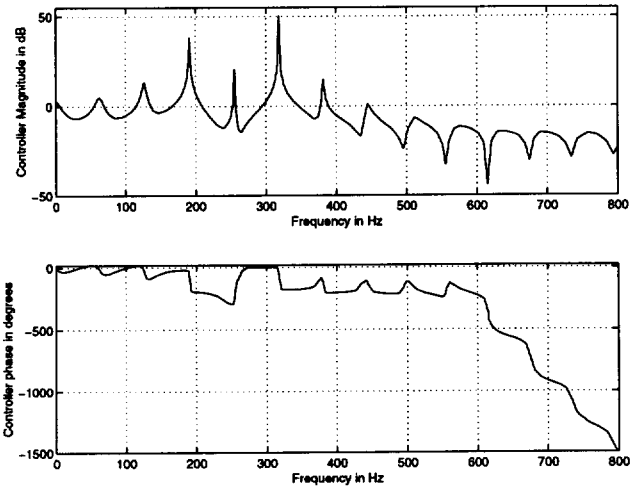

Figure 5: Bode plot of the adapted controller for a dual-tone disturbance (190 Hz, 320 Hz).

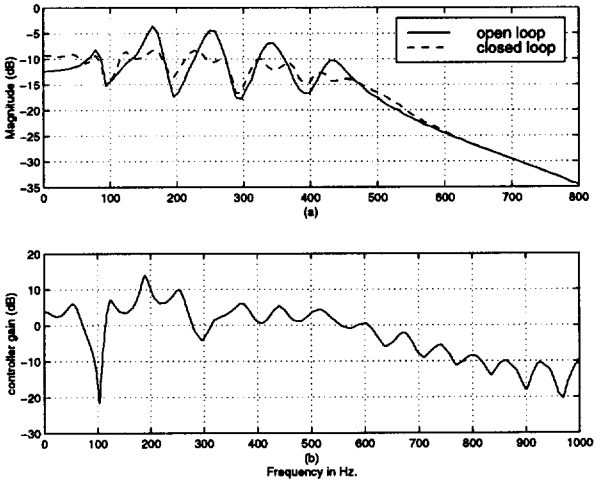

Figure 6: (a) open-loop (G_{zw}) and closed loop ($\tilde{G}_{zw}$) magnitude plots for a broadband disturbance (b) Magnitude plot of the adapted controller for a broadband disturbance.

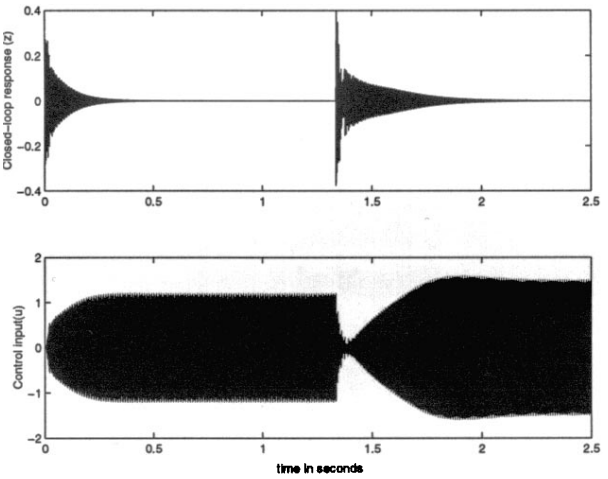

Figure 7: Single-Tone disturbance with frequency change at $t \approx 1.3$.

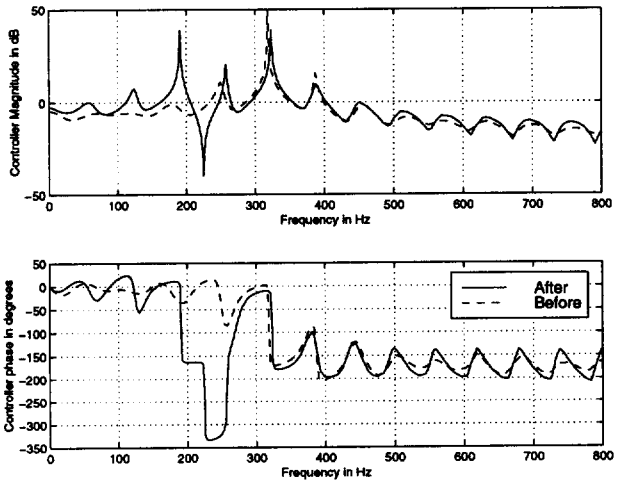

Figure 8: Magnitude plot of the adapted controller before and after the single-tone frequency change.

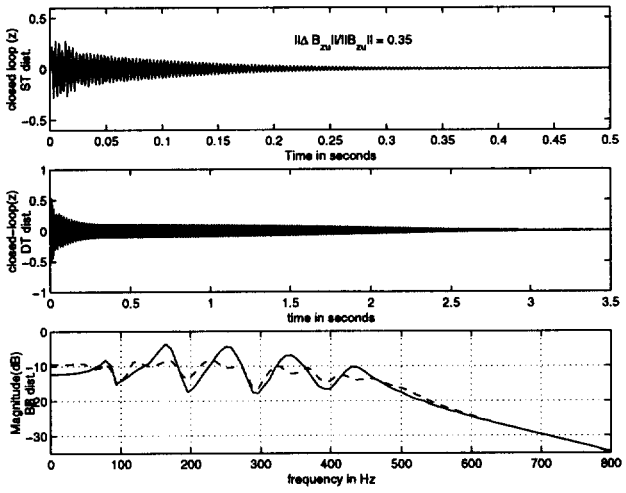

Figure 9: Perturbed B_{zu}: Simulation with $\pm 20\%$ errors in the secondary path matrix B_{zu}.

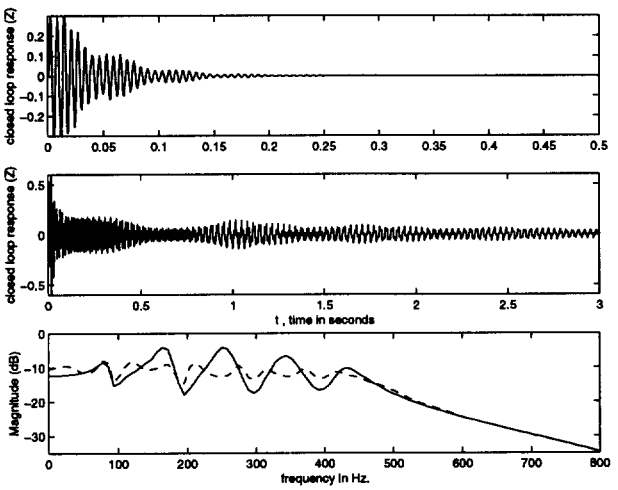

Figure 12: Simulation with a B_{zu} model for a lower order plant.

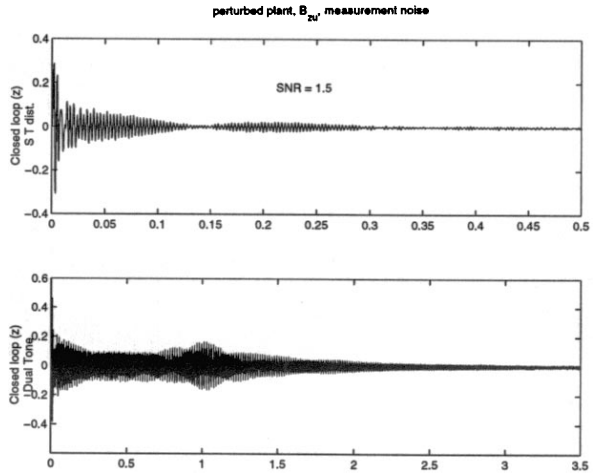

Figure 10: Simulation with perturbed plant and additive Gaussian measurement noise.

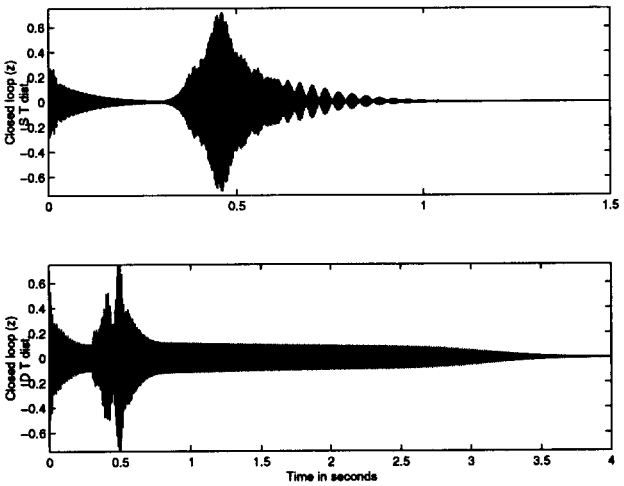

Figure 13: Stabilization and disturbance rejection: Change in feedback sign of the loop transfer function G_{yu}.

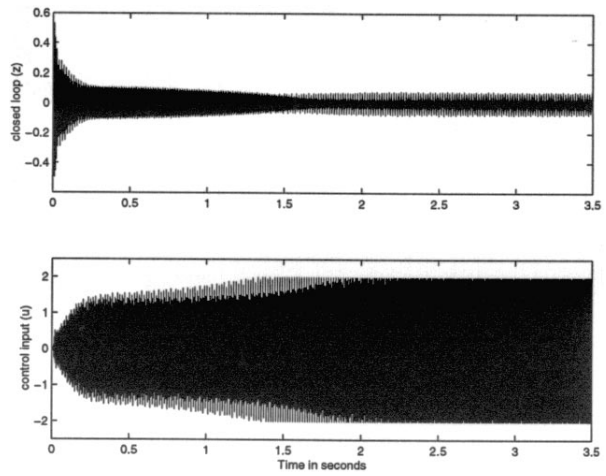

Figure 11: Simulation with noise and control input saturation.

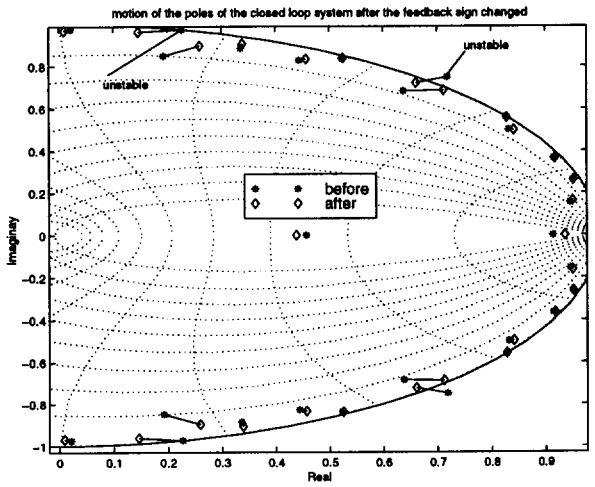

Figure 14: Closed-loop poles just before and after the change in sign of G_{yu}.